A DISCRETE SCHEME FOR PARAMETRIC ANISOTROPIC SURFACE DIFFUSION

FRANK HAUSSER AND AXEL VOIGT

ABSTRACT. In this note we present, how anisotropic surface energies may be incorporated into the finite element method for parametric surface diffusion given by Bänsch et al. [2]. We present the adapted variational formulation, and the resulting semi-implicit discretization. Finally several simulations with strong (convex) anisotropies are shown, where the corresponding Wulff shapes are approached as the steady state.

1. Introduction

A surface $\Gamma(t)$ is evolving according to anisotropic surface diffusion if the normal velocity v satisfies the 4^{th} order parabolic equation

$$v = \Delta_\Gamma \kappa_\gamma \qquad \text{on} \quad \Gamma(t), \tag{1}$$

where Δ_Γ denotes the Laplace-Beltrami operator on $\Gamma(t)$ and κ_γ its anisotropic mean curvature, which may be derived formally as the first variation of the anisotropic surface energy. The notion of surface diffusion goes back to Mullins[8] appearing in the context of material science. Consider a crystal surface, whose dynamic is diffusion dominated, i.e., the morphological evolution does not happen via attachment and detachment of atoms but rather by atoms moving along the surface. Then, the atomic flux J_Γ on the surface is assumed to be proportional to the surface gradient of the chemical potential κ_γ, and the continuity equation $v = -\Omega \nabla_\Gamma J_\Lambda$, Ω denoting the atomic volume, takes the form (1).

In this article, we discuss the incorporation of anisotropy into the finite element method for isotropic surface diffusion of parametric surfaces by Bänsch et al. [2]. Here the starting point is a second order splitting of (1), where the vector valued mean curvature $\vec{\kappa} := \kappa \vec{n}$, appearing as an additional unknown, is expressed as the Laplace-Beltrami of the position vector [7]. A semi-implicit time discretization and integration by parts leads to a weak formulation of the second order system, which is discretized in space using linear finite elements. We will incorporate anisotropy into this scheme by using an appropriate weak formulation for the vector valued anisotropic mean curvature $\kappa_\gamma \vec{n}$, see e.g. [4, 5].

2. Model and Notations

In this section we fix our notation and present some basic differential geometric results. For more details and references to the subject see [10, 5]. Let $\Gamma \subset \mathbb{R}^3$ denote a smooth closed hypersurface with normal vector field $\vec{n}$. In

Date: November 1, 2005.

Key words and phrases. surface diffusion, anisotropy, parametric finite elements.

the following we assume all functions and vector fields to be defined in a neighborhood of Γ. The tangential gradient $\nabla_\Gamma f$ of a function f and the tangential divergence $\nabla_\Gamma \cdot \vec{v}$of a vector field $\vec{v}$ are given by

$$\nabla_\Gamma f = \nabla f - (\vec{n}\cdot\nabla f)\vec{n}, \qquad \underline{\partial}_i f := \big(\nabla_\Gamma f\big)_i = \partial_i f - (\vec{n}\cdot\nabla f)n_i,$$
$$\nabla_\Gamma \cdot \vec{v} = \mathrm{tr}(\nabla_\Gamma \vec{v}) = \sum_i \underline{\partial}_i v_i,$$

where tr denotes the trace in $\mathbb{R}^3$. The Laplace Beltrami operator on Γ may then be expressed as

$$\Delta_\Gamma f = \nabla_\Gamma \cdot \nabla_\Gamma f = \sum_i \underline{\partial}_i \underline{\partial}_i f.$$

The mean curvature κ is the trace of the shape operator $S = \nabla_\Gamma \vec{n}$, or, equivalently the tangential divergence of the surface normal:

$$\kappa = \mathrm{tr}(S) = \nabla_\Gamma \cdot \vec{n}. \tag{2}$$

Also we recall the formula

$$\Delta_\Gamma \vec{x} = -\kappa\vec{n}, \tag{3}$$

which is obtained from (2) using the identity $\underline{\partial}_j x_k = \delta_{jk} - n_j n_k$ for the coordinate functions x_k. Eq. (3) is the starting point of a finite element discretization of mean curvature flow of parametric surfaces in [7], since by integration by parts it implies

$$\int_\Gamma \kappa\vec{n}\cdot\vec{\phi}\,dA = \int_\Gamma \nabla_\Gamma\vec{x}\cdot\nabla_\Gamma\vec{\phi}\,dA \tag{4}$$

Alternatively, the curvature κ may be obtained as the first variation of the surface energy $E[\Gamma] := \int_\Gamma 1 dA$ with respect to normal variations. In terms of a physical interpretation, $E[\Gamma]$ is the surface free energy and κ is the (local) chemical potential μ, describing the rate of change of the free energy when moving the surface in normal direction.

The notion of anisotropic mean curvature is most naturally obtained by introducing an anisotropic surface energy density γ depending on the orientation of the surface Γ. Thus, γ is a smooth function $S^2 \to \mathbb{R}^+$, which may be assumed to be given as a function on $\mathbb{R}^3 - \{0\}$, being positively homogeneous of degree 1. In particular this implies for the second derivative (where we use the symbol D for differentiating with respect to $z \in \mathbb{R}^3$ not to be confused with a point in space)

$$D^2\gamma(z)\cdot z = 0,$$

and therfore $D^2\gamma$ can be interpreted as an endomorphism on the tangent space of Γ. The first variation of the surface energy $E_\gamma[\Gamma]$

$$E_\gamma[\Gamma] = \int_\Gamma \gamma(\vec{n})dA,$$

will be called the anisotropic mean curvature κ_γ and is given by

$$\kappa_\gamma := \mathrm{tr}(D^2\gamma \circ S) = \nabla_\Gamma \cdot D\gamma.$$

Note that in the above definition, γ and $D\gamma$ are evaluated at $z = \vec{n}(\vec{x})$. $D\gamma(\vec{n})$ is called the Cahn-Hoffman vector. To ensure, that the surface energy E_γ is a convex functional – which ensures a well defined gradient flow with respect to this functional – we make the following convexity assumption on γ (for some $\gamma_0 > 0$)

$$D^2\gamma(p)q \cdot q \geq \gamma_0 q \cdot q; \quad \text{for all} \quad p, q \in \mathbb{R}^3, \quad |p| = 1, p \cdot q = 0.$$

Associated with an anisotropy γ is the Wulff shape $\mathcal{W}_\gamma$, defined as

$$\mathcal{W}_\gamma = \{z \in \mathbb{R}^3 | z \cdot q \leq \gamma(z) \text{ for all } q \in \mathbb{R}^3\}.$$

If γ is convex, $\mathcal{W}_\gamma$ is convex and the boundary of $\mathcal{W}_\gamma$ may be parameterized over S^2 using the Cahn-Hoffmann vector, i.e. $S^2 \to \partial\mathcal{W}_\gamma \subset \mathbb{R}^3, \quad \vec{n} \mapsto D\gamma(\vec{n})$ [3].

For a fixed volume, the boundary of the (rescaled) Wulffshape is the unique minimizer of the surface energy (2) [12]. Moreover, the anisotropic mean curvature is constant on the boundary of the Wulff shape [9].

An analog of Eq. (4) for the anisotropic case reads (cf. [4, 5])

$$\int_\Gamma \kappa_\gamma \vec{n} \cdot \vec{\phi}\, dA = \int_\Gamma \gamma(\vec{n}) \nabla_\Gamma \vec{x} \cdot \nabla_\Gamma \vec{\phi}\, dA - \sum_{k,l=1}^{3} \int_\Gamma \gamma_{z^k}(\vec{n}) n_l \nabla_\Gamma x_k \cdot \nabla_\Gamma \phi_l dA, \tag{5}$$

where we have used the notation $\gamma_{z_k} := D_k\gamma$. In particular note, that no second derivative of γ is involved in this weak form. Again this identity is the starting point of a finite element discretization of anisotropic mean curvature flow of parametric surfaces, see [4, 5] and will be used in the next section.

A surface $\Gamma(t)$ is evolving according to anisotropic surface diffusion if the normal velocity v satisfies the following 4^{th} order parabolic equation

$$v = \Delta_\Gamma \kappa_\gamma \qquad \text{on} \quad \Gamma(t).$$

We note that this evolution has the following geometric properties: if $\Gamma(t)$ is a closed surface, then the volume of the bounded domain is preserved and the total energy E_γ decreases. In particular, the boundary of the Wulff shape is a stable steady state. Except for the isotropic case, there are no existence or uniqueness results for this highly nonlinear equation.

3. Variational formulation and finite element discretization

In view of the identity (5), we start as in the isotropic case [2, 7] by rewriting Eq. (1) as a system of 2^{nd} order equations. Using the position vector $\vec{x}$, the curvature vector $\vec{\kappa}_\gamma = \kappa_\gamma \vec{n}$, and the velocity vector $\vec{v} = v\vec{n}$, (1) becomes equivalent to the following system of equations for $\vec{\kappa}_\gamma$, κ_γ, v, and $\vec{v}$

$$(\vec{\kappa}_\gamma)_i = -\nabla_\Gamma \cdot \gamma(\vec{n}) \nabla_\Gamma x_i + \sum_{k=1}^{3} \nabla_\Gamma \cdot \left(\gamma_{z_k} n_i \nabla_\Gamma x_k\right), \quad i = 1, 2, 3 \tag{6}$$

$$\kappa_\gamma = \vec{\kappa}_\gamma \cdot \vec{n}, \tag{7}$$

$$v = \Delta_\Gamma \kappa_\gamma \tag{8}$$

$$\vec{v} = v\vec{n}. \tag{9}$$

Let $\Gamma(t)$ denote the interface at time t. Now split the time interval by discrete time instants $0 = t_0 < t_1 < \dots$ and define time steps $\tau_m := t_{m+1} - t_m$. We represent the next interface $\Gamma^{m+1} = \Gamma(t_{m+1})$ in terms of $\Gamma^m = \Gamma(t_m)$ by updating the position vector

$$\vec{x}^{m+1} \leftarrow \vec{x}^m + \tau_m \vec{v}. \tag{10}$$

In the time discretization, all geometric quantities such as $\vec{n}$ and ∇_Γ are evaluated on the current interface Γ^m, i.e. they are treated explicitly and we end up with a linear system of equations. In contrast to the geometric quantities, the unknowns $\vec{\kappa_\gamma}$, κ_γ, v, and $\vec{v}$ may be treated implicitly. In Eq. (6), the first term on the right hand side will be treated implicitly, whereas we treat the second term explicitly. Thus, in view of (10), when evaluating $\vec{\kappa}_\gamma^{m+1}$ in Eq. (6), the first term is evaluated at $\vec{x}^{m+1} = \vec{x}^m + \tau_m \vec{v}^{m+1}$, whereas the second term is evaluated at $\vec{x}^m$.

To derive a weak formulation, we proceed as in [2, 7]: multiply (6),(7), (8) and (9) by test functions $\vec{\psi} \in \vec{H}^1(\Gamma)$ and $\psi \in H^1(\Gamma)$, and use integration by parts for the tangential divergence ∇_Γ. For simplicity, we have hereafter dropped the superscript $m+1$ for the unknowns $\vec{\kappa}_\gamma^{m+1}$, etc. Furthermore, using the notation $\langle \cdot, \cdot \rangle$ for the L^2 inner product over the current interface Γ^m, we arrive at the following set of semi-implicit equations:

Problem 1. *For $m = 1, 2, \dots$ find $\vec{\kappa_\gamma} \in \vec{H}^1(\Gamma^m)$, $\kappa_\gamma \in H^1(\Gamma^m)$, $v \in H^1(\Gamma^m)$, and $\vec{v} \in \vec{H}^1(\Gamma^m)$ such that $\forall \psi \in H^1(\Gamma^m)$ and $\forall \vec{\psi} \in \vec{H}^1(\Gamma^m)$*

$$\langle \vec{\kappa_\gamma}, \vec{\psi} \rangle - \tau_m \langle \gamma(\vec{n}) \nabla_\Gamma \vec{v}, \nabla_\Gamma \vec{\psi} \rangle = \langle \gamma(\vec{n}) \nabla_\Gamma \vec{x}^m, \nabla_\Gamma \vec{\psi} \rangle - \sum_{k,l=1}^{3} \langle \gamma_{z_k}(\vec{n}) n_l \nabla_\Gamma x_k^m, \nabla_\Gamma \psi_l \rangle$$

$$\begin{aligned} \langle \kappa_\gamma, \psi \rangle - \langle \vec{\kappa}_\gamma \cdot \vec{n}, \psi \rangle &= 0, \\ \langle v, \psi \rangle + \langle \nabla_\Gamma \kappa_\gamma, \nabla_\Gamma \psi \rangle &= 0, \\ \langle \vec{v}, \vec{\psi} \rangle - \langle v \vec{n}, \vec{\psi} \rangle &= 0. \end{aligned}$$

As compared to the isotropic case, the anisotropy function $\gamma(\vec{n})$ introduces an additional non-linearity, which is treated in an explicit way. Thus the system may no longer be expected to be unconditionally stable in contrast to the isotropic case, where this has been shown in [2]. Therefore, similar as in [6], we add a stabilizing term to the left hand side of the first equation in Problem 1. From numerical experiments it turned out, that the following term is a good candidate:

$$-\tau_m \lambda \Big(\langle \gamma(\vec{n}) \nabla_\Gamma (\vec{v} - \vec{v}^m), \nabla_\Gamma \vec{\psi} \rangle + \sum_{k,l=1}^{3} \langle \gamma_{z_k}(\vec{n}) n_l \nabla_\Gamma (v_k - v_k^m), \nabla_\Gamma \psi_l \rangle \Big). \tag{11}$$

Now the discretization in space is straightforward: Consider a polygonal curve Γ_h^m approximating Γ^m. The polygonal segments are thought of as finite elements. Also for the polygonal curve, we denote by $\vec{n}$ the outer unit normal to Γ_h^m, which may be discontinuous across inter-element boundaries. Denote by $\mathbb{W}_h^m \subseteq H^1(\Gamma_h^m)$ the finite element space of globally continuous, piecewise linear functions with corresponding nodal basis functions $(\psi_l)_{l=1}^L$, where L is

the number of degrees of freedom. By $\vec{\mathbb{W}}_h^m \subseteq \vec{H}^1(\Gamma_h^m)$ we denote the finite element space of vector valued functions with nodal basis functions $(\vec{\psi}_l^q)_{l=1,\dots,L}^{q=1,2,3}$, where $\vec{\psi}_l^q = \psi_l \vec{e}_q$ with ψ_l the scalar basis function defined above and $(\vec{e}_1, \vec{e}_2, \vec{e}_3)$ the standard basis in $\mathbb{R}^3$. Problem 1 is discretized by expanding the functions $\vec{\kappa}_\gamma$, κ_γ, v, $\vec{v}$ in terms of the basis functions and testing against all discrete test functions, i.e. solving Problem 1 in the finite dimensional spaces $\mathbb{W}_h^m$, $\vec{\mathbb{W}}_h^m$.

To arrive at an algorithm in matrix form, expand the unknowns

$$\vec{\kappa}_\gamma = \sum_{l=1}^{L} \vec{K}_l \psi_l, \quad \kappa_\gamma = \sum_{l=1}^{L} K_l \psi_l, \quad \vec{v} = \sum_{l=1}^{L} \vec{V}_l \psi_l, \quad v = \sum_{l=1}^{L} V_l \psi_l$$

for some

$$\begin{aligned} \vec{K} &= (\vec{K}_1, \dots, \vec{K}_L)^t \in \mathbb{R}^{3\times L}, \quad K = (K_1, \dots, K_L)^t \in \mathbb{R}^L \\ \vec{V} &= (\vec{V}_1, \dots, \vec{V}_L)^t \in \mathbb{R}^{3\times L}, \quad V = (V_1, \dots, V_L)^t \in \mathbb{R}^L \end{aligned}$$

and define the mass, stiffness, and normal matrices $\boldsymbol{M}$, $\boldsymbol{A}$, $\boldsymbol{B}$, $\boldsymbol{C}$, $\boldsymbol{N}$ with matrix entries

$$\begin{aligned} M_{kl} &= \langle \psi_k, \psi_l \rangle; \qquad \vec{M}_{kl} = (M_{kl}^{qr}) = (\delta_{qr} M_{kl}) \\ A_{kl} &= \langle \nabla_\Gamma \psi_k, \nabla_\Gamma \psi_l \rangle; \\ B_{kl} &= \langle \gamma(\vec{n}) \nabla_\Gamma \psi_k, \nabla_\Gamma \psi_l \rangle; \qquad \vec{B}_{kl} = (B_{kl}^{qr}) = (\delta_{qr} B_{kl}) \\ C_{kl}^{qr} &= \langle \gamma_{z_r}(\vec{n}) n_q \nabla_\Gamma \psi_k, \nabla_\Gamma \psi_l \rangle; \qquad \vec{C}_{kl}^{qr} = (C_{kl}^{qr}); \\ \vec{N}_{kl} &= (N_{kl}^q) = \langle \psi_k, \psi_l n_q \rangle \end{aligned}$$

where the index ranges are $1 \le k, l \le L$ and $1 \le q, r \le 3$, $\delta_{qr} = \vec{e}_q \cdot \vec{e}_r$ is the Kronecker symbol, and $n_q = \vec{n} \cdot \vec{e}_q$ is the q-th spatial component of the normal.

The following algorithm is the matrix form of the discretized Problem 1:

Algorithm 2. *Find $\vec{K}, \vec{V} \in \mathbb{R}^{3\times L}$, $K, V \in \mathbb{R}^L$ such that*

$$\begin{pmatrix} \vec{\boldsymbol{M}} & \boldsymbol{0} & \boldsymbol{0} & -\vec{\boldsymbol{N}} \\ \boldsymbol{0} & \boldsymbol{M} & -\vec{\boldsymbol{N}}^t & \boldsymbol{0} \\ -\tau_m\big(\vec{\boldsymbol{B}} + \lambda(\vec{\boldsymbol{B}} + \vec{\boldsymbol{C}})\big) & \boldsymbol{0} & \vec{\boldsymbol{M}} & \boldsymbol{0} \\ \boldsymbol{0} & \boldsymbol{A} & \boldsymbol{0} & \boldsymbol{M} \end{pmatrix} \begin{pmatrix} \vec{V} \\ K \\ \vec{K} \\ V \end{pmatrix} = \begin{pmatrix} 0 \\ 0 \\ (\vec{\boldsymbol{B}} - \vec{\boldsymbol{C}})\vec{X}^m - \lambda\tau_m(\vec{\boldsymbol{B}} + \vec{\boldsymbol{C}})\vec{V}^m \\ 0 \end{pmatrix}$$

A Schur complement equation for $\vec{K}, V$ reads

$$\boldsymbol{S} \begin{pmatrix} \vec{K} \\ V \end{pmatrix} = \begin{pmatrix} (\vec{\boldsymbol{B}} - \vec{\boldsymbol{C}})\vec{X}^m - \lambda\tau_m(\vec{\boldsymbol{B}} + \vec{\boldsymbol{C}})\vec{V}^m \\ 0 \end{pmatrix},$$

where

$$\begin{aligned} \boldsymbol{S} &= \begin{pmatrix} \vec{\boldsymbol{M}} & \boldsymbol{0} \\ \boldsymbol{0} & \boldsymbol{M} \end{pmatrix} - \begin{pmatrix} -\tau_m\big(\vec{\boldsymbol{B}} + \lambda(\vec{\boldsymbol{B}} + \vec{\boldsymbol{C}})\big) & \boldsymbol{0} \\ \boldsymbol{0} & \boldsymbol{A} \end{pmatrix} \begin{pmatrix} \vec{\boldsymbol{M}} & \boldsymbol{0} \\ \boldsymbol{0} & \boldsymbol{M} \end{pmatrix}^{-1} \begin{pmatrix} \boldsymbol{0} & -\vec{\boldsymbol{N}} \\ -\vec{\boldsymbol{N}}^t & \boldsymbol{0} \end{pmatrix} \\ &= \begin{pmatrix} \vec{\boldsymbol{M}} & -\tau_m\big(\vec{\boldsymbol{B}} + \lambda(\vec{\boldsymbol{B}} + \vec{\boldsymbol{C}})\big)\vec{\boldsymbol{M}}^{-1}\vec{\boldsymbol{N}} \\ \boldsymbol{A}\boldsymbol{M}^{-1}\vec{\boldsymbol{N}}^t & \boldsymbol{M} \end{pmatrix}. \end{aligned}$$

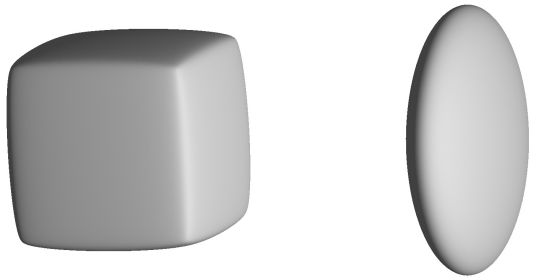

FIGURE 1. Wulffshape $\mathcal{W}_\gamma$ for regularized l^1-anisotropy and disk anisotropy

The above formulation in turn gives rise to the final Schur complement equation for the single unknown V:

$$\begin{aligned}&\big(\tau_m \boldsymbol{A}\boldsymbol{M}^{-1}\vec{\boldsymbol{N}}^t\vec{\boldsymbol{M}}^{-1}\big(\vec{\boldsymbol{B}}+\lambda(\vec{\boldsymbol{B}}+\vec{\boldsymbol{C}})\big)\vec{\boldsymbol{M}}^{-1}\vec{\boldsymbol{N}}+\boldsymbol{M}\big)V\\ &\qquad = \boldsymbol{A}\boldsymbol{M}^{-1}\vec{\boldsymbol{N}}^t\vec{\boldsymbol{M}}^{-1}\big((\vec{\boldsymbol{C}}-\vec{\boldsymbol{B}})\vec{X}^m+\lambda\tau_m(\vec{\boldsymbol{B}}+\vec{\boldsymbol{C}})\vec{V}^m\big).\end{aligned} \tag{12}$$

We note that for $\lambda = 0$, the same arguments as in the isotropic case [1] show that the linear system (12) is uniquely solvable: Introduce the symmetric non-negativ matrix $\boldsymbol{L}$ and denote the matrix in the left-hand side of (12) by $\boldsymbol{T}$

$$\boldsymbol{L} = \vec{\boldsymbol{N}}^t\vec{\boldsymbol{M}}^{-1}\vec{\boldsymbol{B}}\vec{\boldsymbol{M}}^{-1}\vec{\boldsymbol{N}}, \qquad \boldsymbol{T} = \tau_m\boldsymbol{A}\boldsymbol{M}^{-1}\boldsymbol{L}+\boldsymbol{M}.$$

It is enough to show, that if $\boldsymbol{T}V = 0$ then V must be 0. Now, assuming $\boldsymbol{T}V = 0$ implies $V^t\boldsymbol{L}\boldsymbol{M}^{-1}\boldsymbol{T}V = 0$. Thus, we obtain

$$0 = \tau_m V^t\boldsymbol{L}\boldsymbol{M}^{-1}\boldsymbol{A}\boldsymbol{M}^{-1}\boldsymbol{L}V + V^t\boldsymbol{L}V \geq 0,$$

by symmetry and non-negativity of the involved matrices. It follows that $V^t\boldsymbol{L}V = 0$, implying $\boldsymbol{L}V = 0$. Thus, we obtain $\boldsymbol{M}V = \boldsymbol{T}V$. Since $\boldsymbol{M}$ is invertible we finally conclude that $\boldsymbol{T}V = 0$ implies $V = 0$.

Once the scalar velocity V is obtained by solving (12), the unknown $\vec{V}$ is easily computed by solving $\vec{\boldsymbol{M}}\vec{V} = \vec{\boldsymbol{N}}V$, and then $\vec{X}$ is updated through

$$\vec{X} \leftarrow \vec{X} + \tau_m\vec{V}.$$

4. Implementation and results

In this section, we present some numerical results. To test the proposed method, we chose the following two strong (convex) anisotropies

$$\gamma(z) = \sum_{k=1}^{3}(\varepsilon|z|^2 + z_k^2)^{\frac{1}{2}}, \quad \varepsilon = 0.01 \qquad \text{(regularized } l^1\text{-anisotropy)} \tag{13}$$

$$\gamma(z) = (\alpha z_1^2 + z_3^2 + z_3^2)^{\frac{1}{2}}, \quad \alpha = 0.1 \qquad \text{(disk anisotropy)} \tag{14}$$

The corresponding Wulffshapes $\mathcal{W}_\gamma$ are depicted in Fig. 1. We investigate the evolution of a sphere with volume $V = 1.0$ to the corresponding Wulff shape as the steady state solution of eq. (1). In all simulations, the stabilization parameter $\lambda = 1$. The numerical method is implemented in AMDiS [11]. In each time step, the non symmetric system (12) is solved using a GMRES-Solver.

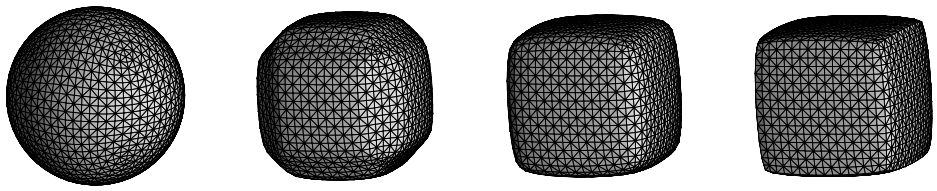

FIGURE 2. Evolution of a sphere with volume $V = 1.0$ towards its steady state with anisotropy (13). No space/time adaptivity: 1538 grid points and time step $\tau = 10^{-5}$. The surface is shown at times $t = 0$, $t = 2 \times 10^{-4}$, $t = 5 \times 10^{-4}$, $t = 10^{-3}$. Note that the rounded corners of the Wulff shape in Fig. 1 are not properly resolved in the steady state ($t = 10^{-3}$) since the spatial discretization is not fine enough.

We use a local mesh regularization and angle width control to prevent mesh distortion as well as time step control and adaptivity in space along the lines as described by Bänsch et al in [2], which will be shortly reviewed below.

As a first example, we present a simulation without using space/time adaptivity in Fig. 2. The time evolution of a sphere using the regularized l^1-anisotropy given in (13) approaches a steady state at $t \approx 10^{-3}$. Comparing with Fig. 1, it reveals that the rounded corners of the Wulff shape are not resolved properly.

Therefore we use adaptivity in space to resolve the zones of high curvature appropriately. However, decreasing the local mesh size considerably, we are forced to use smaller time steps when the evolution of the surface is fast. Thus, to increase the computational accuracy we use a time step control enforcing small time steps whenever the dynamics is fast and/or the normal velocity exhibits large variations and allow large time steps otherwise. The dynamics is measured by the position change of a node given by τv. In view of eq. (10) the relative position change of two nodes in an element with mesh size h tangential to Γ is bounded by $C\tau h|\nabla_\Gamma \vec{v}|$, with C being a mesh independent constant. Thus, to ensure that the position change of a node in tangential and in normal direction does not exceed a fraction of the local mesh size h, we chose two parameters α_t, β_t and require

$$\tau < \alpha_t \big(\max(|\nabla_\Gamma \vec{v}|)\big)^{-1} + \beta_t \big(\max(|v/h|)\big)^{-1}.$$

Moreover, a minimal and a maximal time step is fixed. In all simulations with time step control, we use $\alpha_t = \beta_t = 0.01$, $\tau_{min} = 10^{-8}$, $\tau_{max} = 10^{-5}$. Note, that in [2] $\beta_t = 0$ and $\alpha_t = 0.1$.

Space adaptivity is based on a geometric criterion, as proposed by [2]: here the idea is to assume that the (local) accuracy of the mesh in representing Γ is proportional to $h^2|\nabla_\Gamma \vec{n}|$, where h is the local mesh size and $\nabla_\Gamma \vec{n}$ is the shape operator. Considering two adjacent elements with corresponding normals $\vec{n}_1$,$\vec{n}_2$, $|\nabla_\Gamma \vec{n}|$ at the common edge S may be approximated as

$$h|\nabla_\Gamma \vec{n}| \approx |\vec{n}_1 - \vec{n}_2| =: e_s.$$

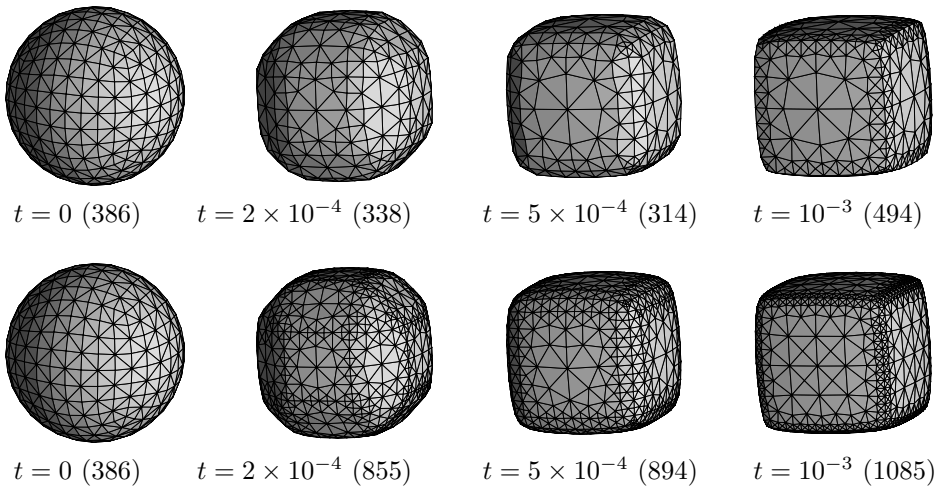

FIGURE 3. Evolution of a sphere with volume $V = 1.0$ towards its steady state with anisotropy (13). Refinement in regions of high curvature and coarsening in nearly flat regions (the number of grid points is given between parentheses). Top row: element tolerance $\varepsilon_s = 0.1$, bottom row: $\varepsilon_s = 0.05$

Thus, for each triangle T, define the local error indicator

$$E_T := \sum_{S \subset T} e_s h.$$

Choosing an element tolerance ε_s and refinement and coarsening parameters $0 < \gamma_r, \gamma_c$, one does proceed as follows: If $\max(E_T) > \varepsilon_s$, all elements with $E_T > \gamma_r$ are refined. In any case all elements with $E_T < \gamma_c$ are coarsened. For details see [2].

Setting $\gamma_c = 0.3$, $\gamma_r = 0.7$, the resulting meshes, for two different values of ε_s are depicted in Fig. 3. As shown in Fig. 4, the rounded corners of the Wulff shape are resolved if the mesh is refined appropriately in the regions of high curvature. In lack of an analytical solution for anisotropic surface

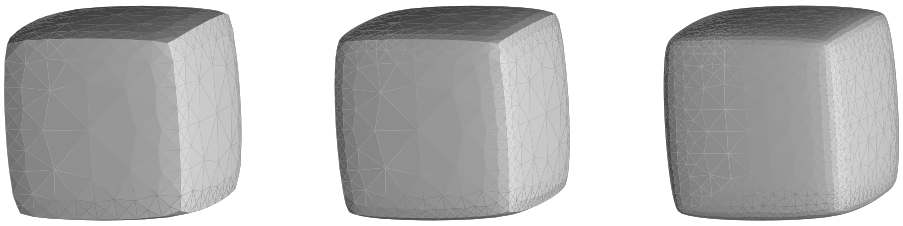

FIGURE 4. Evolution of a sphere with volume $V = 1.0$ towards its steady state with anisotropy (13). Solution at $t = 2 \times 10^{-3}$: (from left to right) element tolerance $\varepsilon_s = 0.1$, 0.05, 0.02. Note that the number of grid points (given between parentheses) in the steady state is roughly proportional to $1/\varepsilon_s$

diffusion of parametric surfaces, we investigate the accuracy and (experimental) convergence of our numerical method as follows: As shown in Fig. 5(left), the volume is conserved within less then 1%. The decay of the surface energy is roughly exponential, and the energy of the steady state approaches the energy of the Wulff shape (with the same volume as the numerical steady state), when increasing the spatial resolution, see Fig. 6. Moreover, also the area of the numerical steady state converges to the area of the Wulff shape as shown in Fig. 5(right).

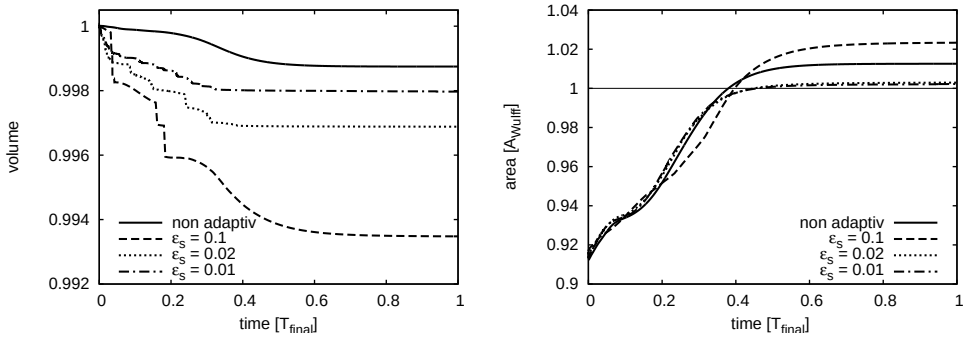

FIGURE 5. Evolution of a sphere with volume $V = 1.0$ towards its steady state with anisotropy (13). (Left) Volume versus relative time t/T_{final} ($T_{\text{final}} = 2 \times 10^{-3}$): the volume is conserved within less then 1% in all simulations. (Right) Relative area A/A_{Wulff} versus relative time, where A_{Wulff} is the area of the Wulff shape with volume $V(T_{\text{final}})$; (for $V = 1$, $A_{\text{Wulff}} \approx 5.3097$). The area of the steady state approaches A_{Wulff} for small ε_s very accurately.

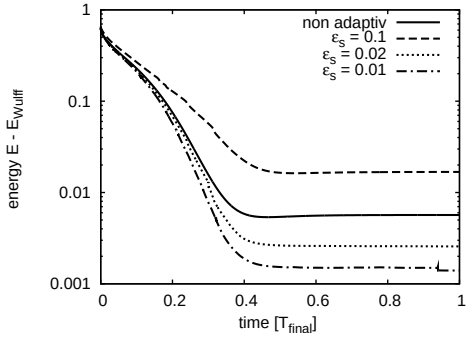

FIGURE 6. Evolution of a sphere with volume $V = 1.0$ towards its steady state with anisotropy (13). Surface energy $E - E_{\text{Wulff}}$, versus relative time, where E_{Wulff} is the surface energy of the Wulff shape with volume $V(T_{\text{final}})$; (for $V = 1$, $E_{\text{Wulff}} \approx 6.8922$). The surface energy decays exponentially and the energy of the steady state approaches E_{Wulff} with decreasing tolerance ε_s.

As a final example we present the evolution of a sphere to the steady state using the disk anisotropy (14). Note that in this case it is even more important to resolve the high curvature zones appropriately, see Fig. 7.

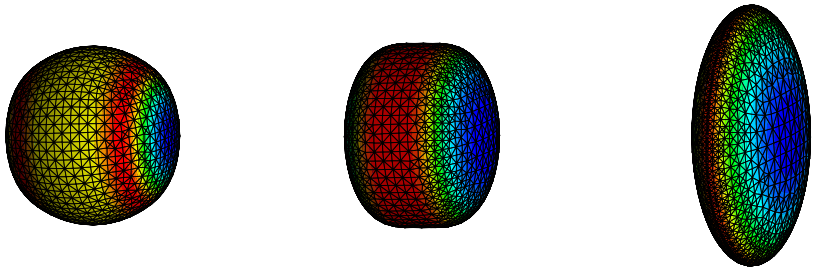

$t = 3 \times 10^{-4}$ (1543) $t = 3 \times 10^{-3}$ (1934) $t = 3 \times 10^{-2}$ (2527).

FIGURE 7. Evolution of a sphere towards its steady state with anisotropy (14) and element tolerance $\varepsilon_s = 0.02$. The number of grid points is given between parentheses. The color-coding indicates the normal velocity (rescaled), ranging from red (maximal outwards) over yellow to blue (maximal inwards)

References

[1] E. Bänsch, F. Haußer, O. Lakkis, B. Li, and A. Voigt. Finite element method for epitaxial growth with attachment-detachment kinetics. *J. Comput. Phys.*, 194:409–434, 2004.

[2] E. Bänsch, P. Morin, and R. H. Nochetto. A finite element method for surface diffusion: the parametric case. *J. Comput. Phys.*, 203:321–343, 2005.

[3] J.W. Cahn and D.W. Hoffman. Vector thermodynamics for anisotropic surfaces 2. curved and faceted surfaces. *Acta metall.*, 22, 1974.

[4] U. Clarenz, G. Dziuk, and M. Rumpf. On generalized mean curvature flow in surface processing. In *Geometric analysis and nonlinear partial differential equations*, pages 217–248. Springer, Berlin, 2003.

[5] K. Deckelnick, G. Dziuk, and C.M.Elliott. Computation of geometric partial differential equations and mean curvature flow. *Acta Numerica*, 2005.

[6] K. Deckelnick, G. Dziuk, and C.M.Elliott. Fully discrete semi-implicit second order splitting for anisotropic surface diffusion of graphs. *SIAM J. Numer. Anal.*, to appear.

[7] G. Dziuk. An algorithm for evolutionary surfaces. *Numer. Math.*, 58:603–611, 1991.

[8] W.W. Mullins. Theory of thermal grooving. *J. Appl. Phys.*, 28(3):333–339, 1957.

[9] J.E. Taylor. Crystalline variational problems. *Bull. Amer. Math. Soc.*, 84(4):568–588, 1978.

[10] J.W. Taylor. Mean curvature and weighted mean curvature. *Acta metall. mater.*, 40(7), 1992.

[11] S. Vey and A. Voigt. AMDiS – adaptive multidimensional simulations: object oriented software concepts for scientific computing. *WSEAS Transactions on Systems*, 3:1564–1569, 2004.

[12] G. Wulff. Zur Frage der Geschwindigkeit des Wachstums und der Auflösung der Kristallflächen. *Zeitschr. F. Kristallog.*, 34:449–530, 1901.

Frank Hausser, Crystal Growth Group, Research Center caesar, Ludwig-Erhard-Allee 2, 53175 Bonn, Germany

E-mail address: hausser@caesar.de

Axel Voigt, Crystal Growth Group, Research Center caesar, Ludwig-Erhard-Allee 2, 53175 Bonn, Germany, and, Institute for Pure and Applied Mathematics, University of California, Los Angeles, 460 Portola Plaza, Los Angeles, CA 90095-7121, USA

E-mail address: voigt@caesar.de